Electronic Supplementary Material (ESI) for Journal of Materials Chemistry A.
This journal is © The Royal Society of Chemistry 2018

Electronic Supplementary Information for

Nitrogen-doped 3D Open-Structured Graphite Nanofiber Matrix for High-Performance Supercapacitors

Yongsheng Zhou [*,a,b], *Yingchun Zhu* [b], *Dongfeng Xue* [c] *and Bingshe Xu* [d]

[a] College of Chemistry and Materials Engineering, Anhui Science and Technology University, Bengbu, 233100, P. R. China

[b] Key Laboratory of Inorganic Coating Materials CAS, Shanghai Institute of Ceramics, Chinese Academy of Sciences, Shanghai, 200050, P. R. China

[c] State Key Laboratory of Rare Earth Resource Utilization, Changchun Institute of Applied Chemistry, Chinese Academy of Sciences, Changchun, 130022, P. R. China

[d] Key Laboratory of Interface Science and Engineering in Advanced Materials, Ministry of Education, Taiyuan University of Technology, Taiyuan, 030024, P. R. China

E-mail: yszhou1981@gmail.com

Methods

Synthesis and N-doping of ordered mesoporous graphite nanofiber (OMGNF-N)

A simplified method was used to obtain N-doped ordered mesoporous graphite nanofiber (OMGNF-N). This is by combining CVD with a sol-gel process containing a sol made of polyethylene glycol (PEG, as an inexpensive pore-forming agent and C source), urea (as an inexpensive N source), magnesium nitrate hexahydrate, and Cobalt(II) acetate tetrahydrate. The gel precursor was first prepared by dissolving $Mg(NO_3)_2 \cdot 6H_2O$ (1.0 g), $Co(Ac)_2 \cdot 4H_2O$ (Ac = acetate) (1.0 g), urea (2.0 g) and PEG (2.5 g) in 10 mL ethanol under vigorous stirring, followed by gelation at 30 °C for 8 h and heating at 80 °C for 4 h. OMGNF-N was grown on the resulting xerogel at 1,000 °C under a gas mixture ($Ar:CH_4:NH_3$=300:10:100 sccm) flow in an induction furnace. The extremely ordered hierarchical porous graphite nanofiber was harvested after the acidic etching of the sample by a hot concentrated HNO_3 solution to remove Co/MgO. The N content was also adjusted by changing the amount of urea. For example, the mass ratio of PEG: urea =1:1 enabled us to obtain OMGNF-N containing 6.9% N; if the ratio increases to 1:2, the content of nitrogen increases to 9.4%.

Characterization of materials

Scanning electron microscope (SEM) images were obtained using an S-4800 field emission scanning electron microscope (Hitachi, Japan) operating at 10 kV. The transmission electron microscope (TEM) images were obtained using a FEI Titan G_2 60-300 operating at 80 kV. Low angle X-ray diffraction (θ-2 θ scan) to determine the superstructure of MBGNTs and MBGNTs-N was performed on a Brucker D8 powder X-ray diffractometer using Cu Kα radiation. Raman spectra were recorded with a Renishaw RM-1000 Micro Raman Spectrometer. Investigations of

chemical compositions were performed using X-ray photoelectron spectroscopy (XPS, Physical Electronics PHI 5600). N_2 sorption analysis was conducted on an ASAP2020 accelerated surface area and porosimetry instrument (Micromeritics), equipped with automated surface area, at 77 K using BarrettEmmettTeller (BET) calculations for the surface area. The pore size distribution (PSD) plot was recorded from the adsorption branch of the isotherm based on the Barrett−Joyner−Halenda (BJH) method.

Electrochemical measurements

Electrochemical experiments were performed in several configurations and electrolytes. For aqueous electrolytes, 1.0 M H_2SO_4 (pH 0), 2.0 M Li_2SO_4 (pH 0.5, 1.8, 9.2), and 6.0 M KOH (pH 14) solutions were used. In three-electrode cells, in addition to the working electrode of active material, platinum as the counter electrode and Ag/AgCl as the reference electrode were used. In symmetric cells, two identical (by weight, size and composition) active-material electrodes were used as cathode and anode. Cyclic voltammetry (CV) tests and galvanostatic charge–discharge (CC) tests were performed using an electrochemical analyzer, CHI 660E, under ambient conditions. Electric impedance spectroscopy (EIS) was performed with an amplitude of 10 mV, from 10 mHz to 100 kHz.

Symmetric devices with two identically configured electrodes were also packaged. Since the electrodes were highly conductive, they were directly connected to the electrochemical analyzer by alligators without any current collector other than the 3D graphene foam that was an integral part of the electrode construction. After inserting an ion-porous separator (Celgard 3501) between the two electrodes, the electrode/electrolyte assembly was wrapped within a Kapton tape seal to complete the package.

The specific capacitance (C for CV curves and Cs for GCD curves, Cs1 for three-electrode and Cs2 for two-electrode configuration), the energy density (E) and the power density (P) of these cells were calculated using the following equations:

a. the calculation of specific capacitance by CV and GCD curves in three-electrode configuration:

$$C = \frac{\int Idv}{S \bullet \Delta V \bullet m} \quad (1)$$

$$C_{s1} = \frac{I}{m \bullet (dV/dt)} \quad (2)$$

Where I (A) is the discharge current, S (V s^{-1}) is the scan rate, dV/dt is the slope of the discharge curve (V s^{-1}), m (g) is the mass of the single working electrode, and ΔV (V) denotes the voltage change excluding the IR drop during the discharge process.

b. the calculation of specific capacitance by CV and GCD curves in two-electrode configuration:

$$C = \frac{\int Idv}{S \bullet \Delta V \bullet m} \quad (3)$$

$$C_{s2} = \frac{2I}{m \bullet (dV/dt)} \quad (4)$$

c. the calculation of energy density (E) and power density (P):

$$E = \frac{C_{s2} \bullet \Delta V^2}{2 \bullet 3.6} \quad (5)$$

$$P = \frac{E \bullet 3600}{\Delta t} \quad (6)$$

Where I (A) is the discharge current, S (V s^{-1}) is the scan rate, dV/dt is the slope of the discharge curve (V s^{-1}), Δt (s) is the discharge time, m (g) is the mass of the single working electrode, and ΔV (V) denotes the voltage change excluding the IR drop during the discharge process.

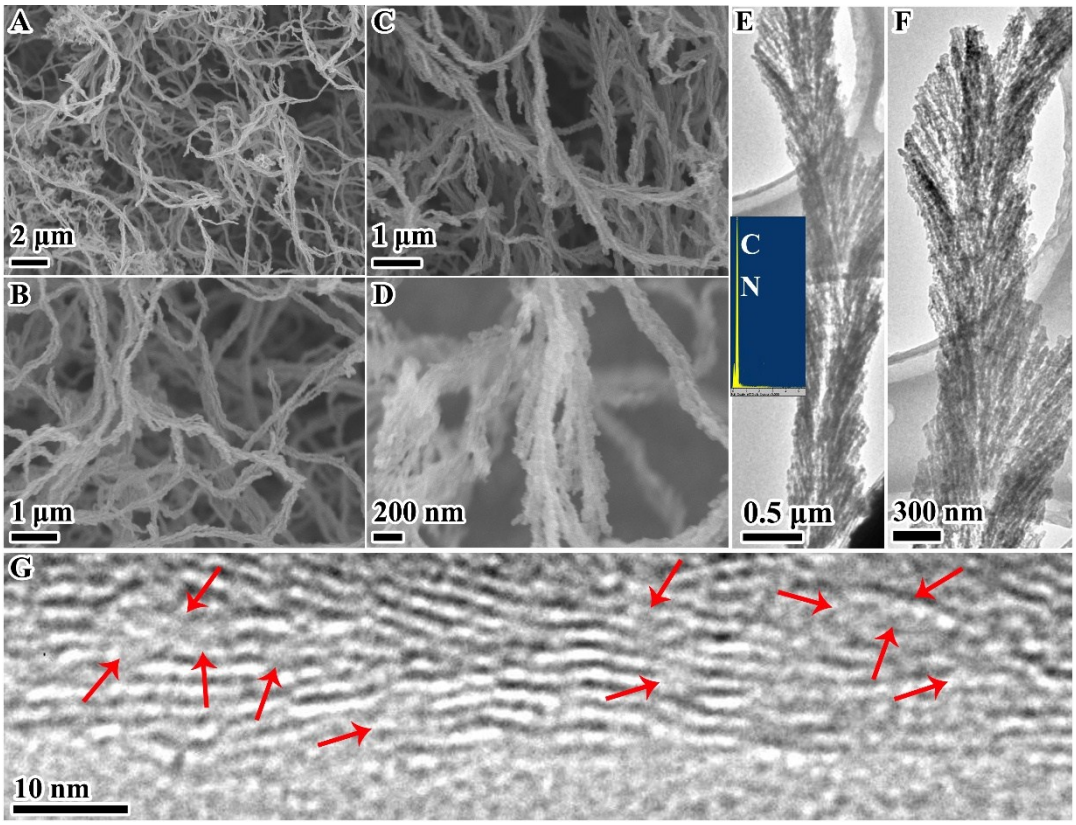

Figure S1. Typical SEM images of the OMGNF-N (A-D). Typical TEM images of the OMGNF-N (E-F) with the inset in (E) showing the corresponding EDS spectrum. (G) HRTEM image of the OMGNF-N.

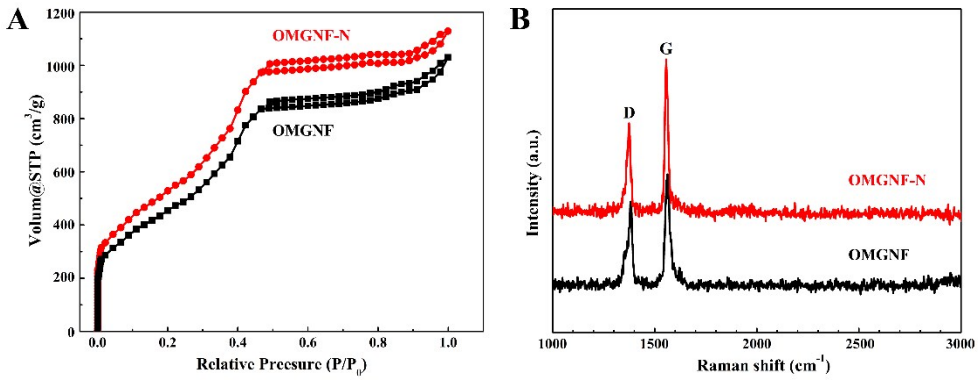

Figure S2. Properties of OMGNF and OMGNF-N. (A) N_2 adsorption−desorption isotherms. All exhibit typical Langmuir hysteresis indicating presence of well-defined mesopores. (B) Raman spectra.

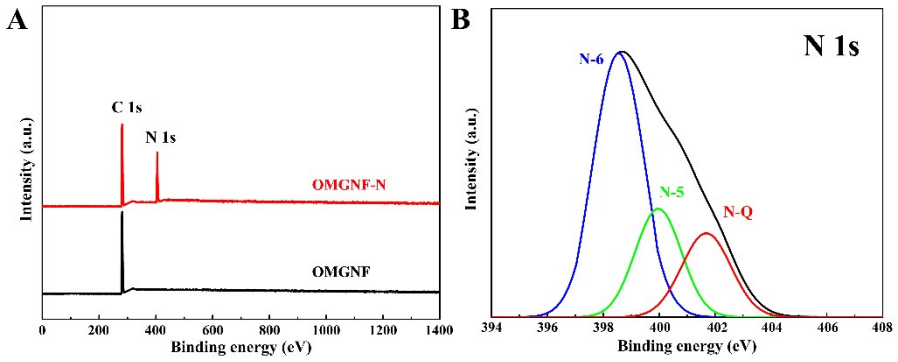

Figure S3. (A) XPS spectra over a wide range of binding energies of OMGNF, and OMGNF-N. (B) The fine-scanned N 1s spectra of OMGNF-N.

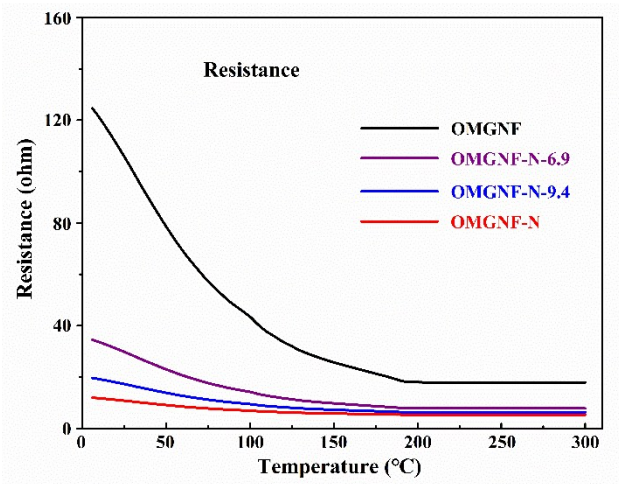

Figure S4. Resistance of OMGNF, OMGNF-N-6.9, OMGNF-N-9.4, and OMGNF-N.

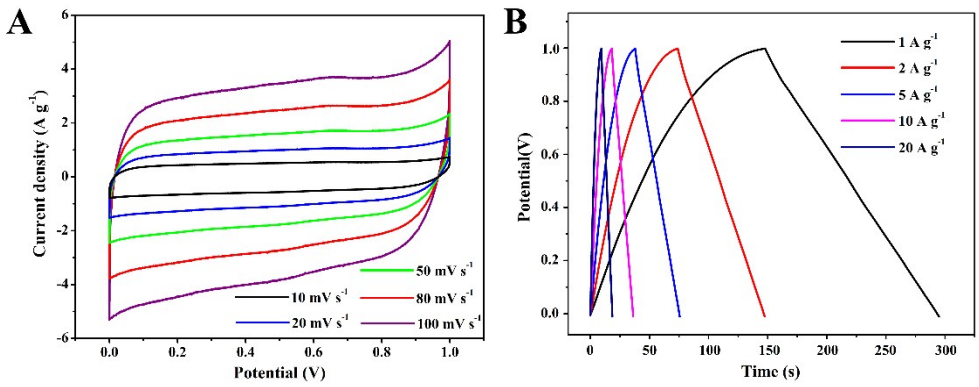

Figure S5. A) and B) CV and GCD curves for OMGNF tested in three-electrode configuration in 6.0 M KOH.

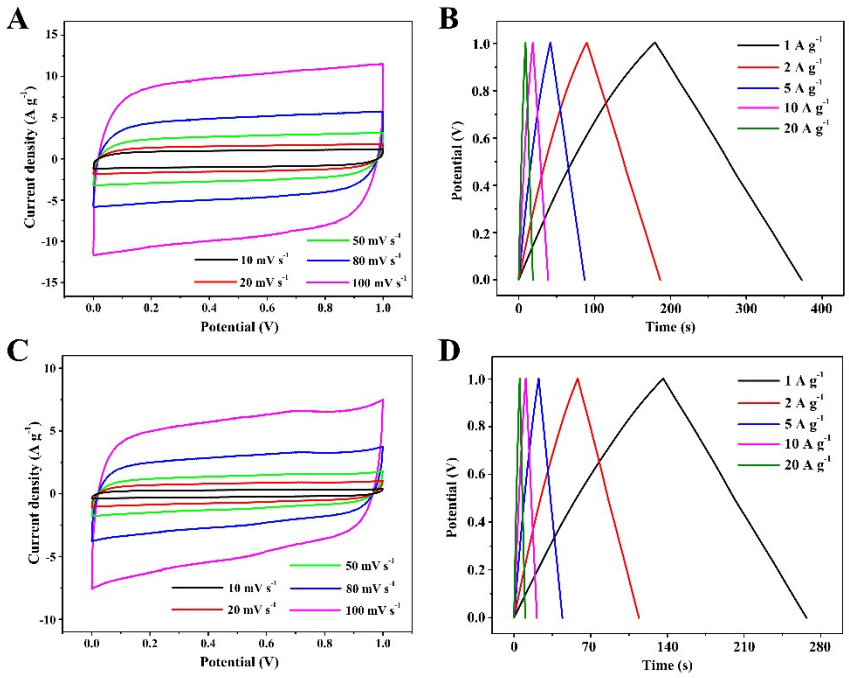

Figure S6. OMGNF-N tested in three-electrode configuration in 6.0 M KOH. (A) CV curves for scan rates of from 10 to 100 mV s^{-1} for OMGNF-N-9.4. (B) GCD curves under different constant currents for OMGNF-N-9.4. (C) CV curves for scan rates of from 10 to 100 mV s^{-1} for OMGNF-N-6.9. (D) GCD curves under different constant currents for OMGNF-N-6.9.

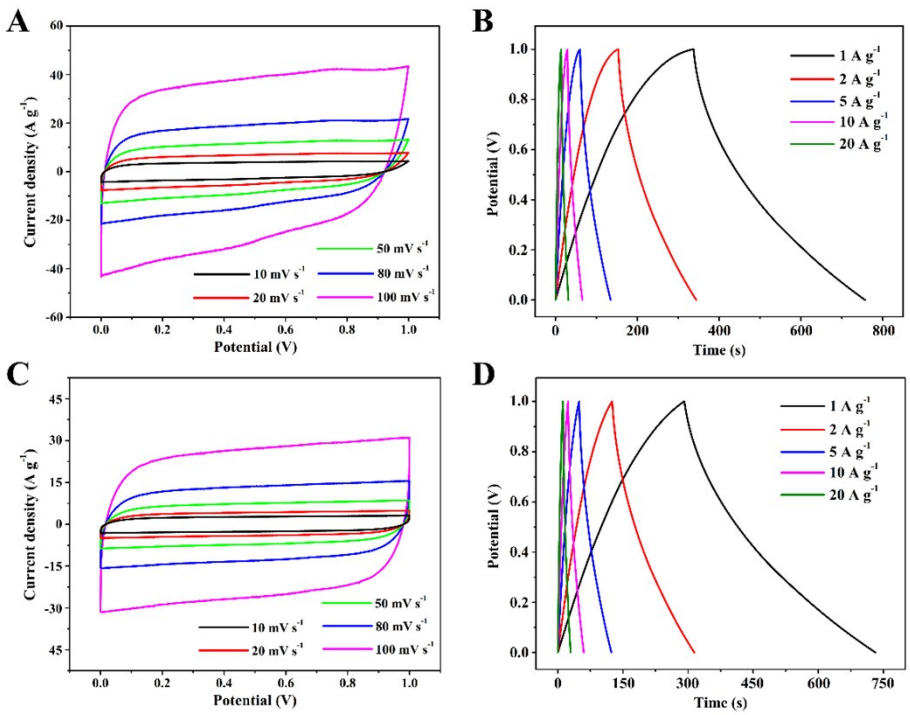

Figure S7. Performances of OMGNF-N with the different area mass loading in three-electrode configuration in 6.0 M KOH. (A) and (B) CV and GCD curves of OMGNF-N with the area mass loading of 0.6 mg cm^{-2}. (C) and (D) CV and GCD curves of OMGNF-N with the area mass loading of 0.8 mg cm^{-2}.

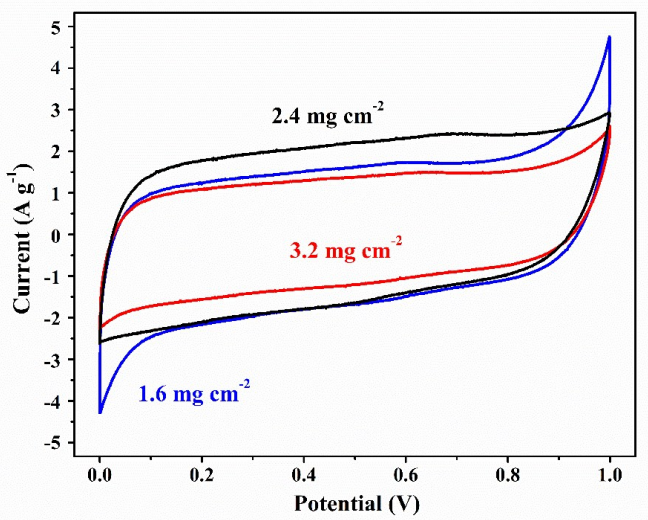

Figure S8. CV curves of OMGNF-N with different area mass loading at the scan rate of 5 mV s^{-1} in three-electrode configuration in 6.0 M KOH.

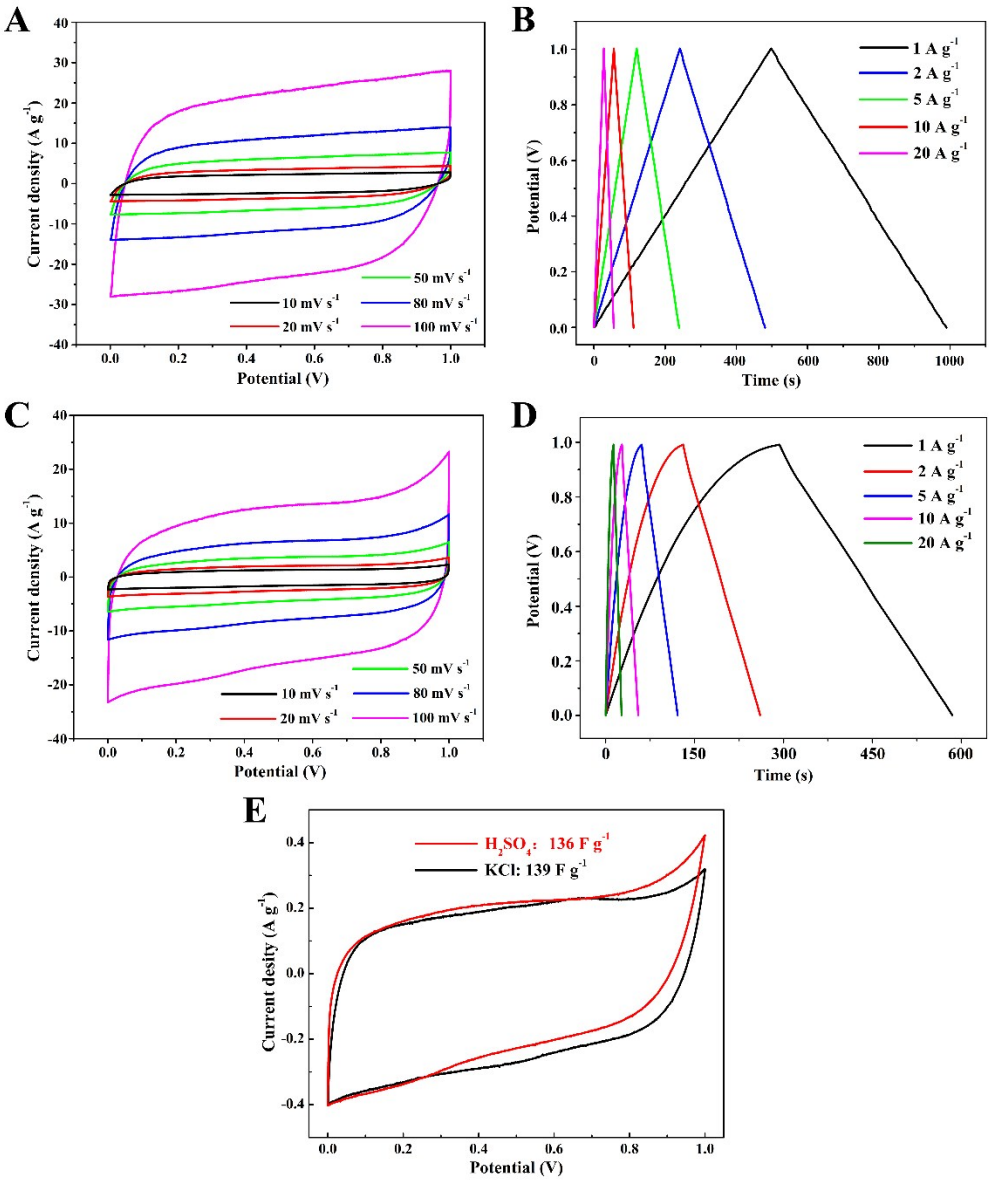

Figure S9. OMGNF-N tested in three-electrode configuration in different electrolyte. (A) CV curves at scan rates of from 10 to 100 mV s^{-1} in 1.0 M H_2SO_4. (B) GCD curves under different constant currents in 1.0 M H_2SO_4. (C) CV curves at the scan rates of from 10 to 100 mV s^{-1} in 1.0 M KCl. (D) GCD curves under different constant currents 1.0 M KCl. (E) CV curves at 10 mV s^{-1} of OMGNF in 1.0 M H_2SO_4 and 1.0 M KCl electrolytes, showing nearly identical capacitance.

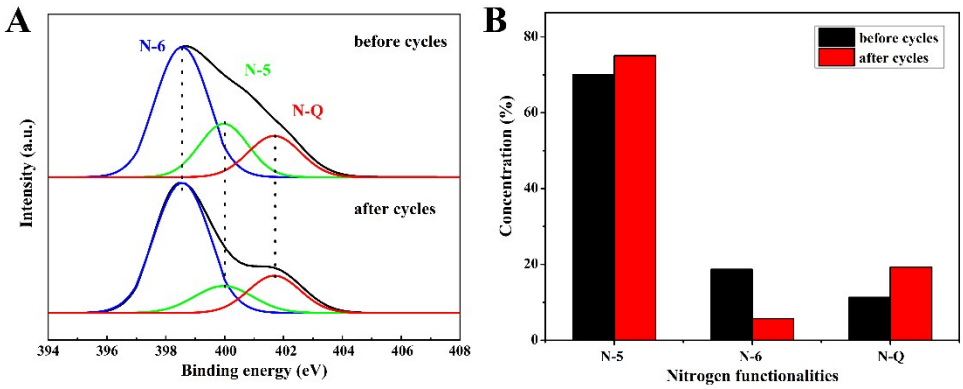

Figure S10. A) Deconvoluted N 1s spectra of OMGNF-N before and after 50000 cycles. B) Concentration distribution of nitrogen groups before and after 50000 cycles.

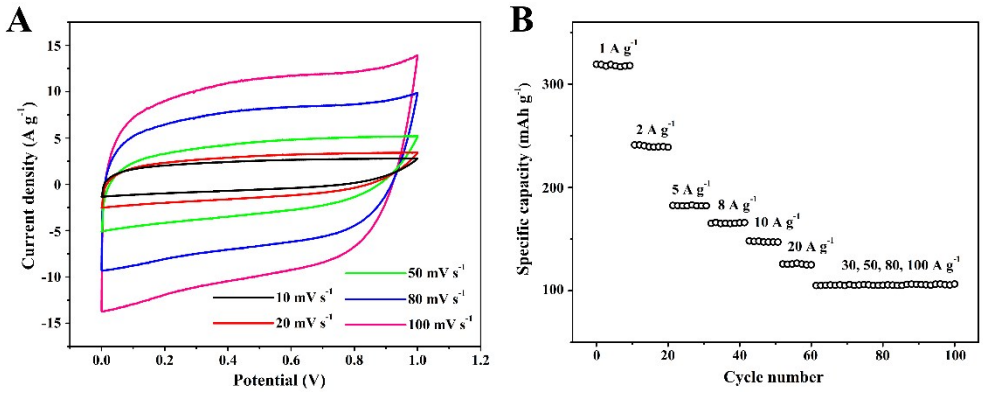

Figure S11. Performances of OMGNF-N tested in two-electrode configuration in H_2SO_4 electrolyte. A) CV curves. B) Specific capacitance at different current densities.

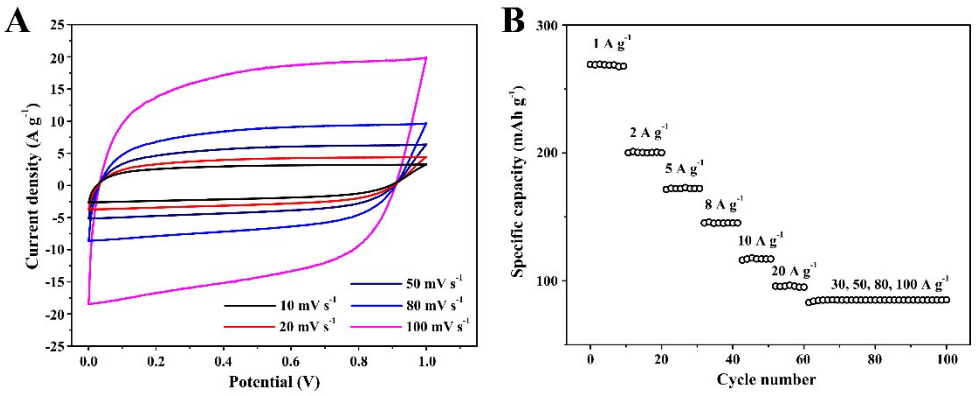

Figure S12. Performances of OMGNF-N tested in two-electrode configuration in KCL electrolyte. A) CV curves. B) Specific capacitance at different current densities.

Table S1. N content in OMGNF-N samples.

Sample	N (at.%)	%N-6†	%N-5†	%N-Q†	%N-5+ %N-6
OMGNF-N	16.5	11.73	2.93	1.84	14.66
OMGNF-N-9.4	9.4	6.01	2.43	0.96	8.44
OMGNF-N-6.9	6.9	4.59	1.55	0.76	6.14

† %N-6, %N-5, and %N-Q are the percentage of "pyridinic" N (N-6), "pyrrolic" N (N-5), and "graphitic" N (N-Q) in OMGNF-N, respectively; see a schematic of these nitrogen locations in Fig. 1B.

Table S2 Selected N-doped carbon based structure for SCs.

Materials	N level (at %)	Electrolyte	Capacitance (F g^{-1}), Test configuration (2 or 3- electrode)	E (Wh kg^{-1}) /P (W kg^{-1})	Ref.
3D honeycomb-like porous carbon	2.85	KOH	68 at 0.2 A g^{-1}, 2 300 at 0.5 A g^{-1}, 3	9.4/96	1
Porous NG/CNTs	4.12	KOH	247 at 0.5 A g^{-1}, 3	N/A	2
Porous N-rich carbon composite	2.3	KOH	240 at 0.1 A g^{-1}, 3	7.07/22.5	3
N-rGO/MWCNTs/NF	N/A	KOH	142 at 1 A g^{-1}, 2	N/A	4
Crumpled NG nanosheets	9.96	KOH	245.9 at 5 mV s^{-1}, 3	N/A	5
N-CNF /rGO/bacterial cellulose	4.82	KOH H_2SO_4	263 at 0.125 A g^{-1}, 3 318 at 0.125 A g^{-1}, 3	N/A	6
NG hydrogel	9.64	KOH	190.1 at 10 A g^{-1}, 2	23.8/9000	7
Ice-templated NG	6.2	KOH	217 at 5 mV s^{-1}, 3	N/A	8
porous carbon nanosheets	1.1	KOH	350 at 0.1 A g^{-1}, 2	22.8/198.8	9
porous mycelium-derived activated carbon	N/A	H_2SO_4	190 at 1 A g^{-1}, 2	N/A	10
porous few-layer carbon	1.52	H_2SO_4	340 at 0.5 A g^{-1}, 3	8.33/6000	11
hierarchal carbon fiber web	N/A	H_2SO_4	298 at 1 A g^{-1}, 3	N/A	12
Our work	16.5	KOH H_2SO_4 KCl	426 at 1 A g^{-1}, 2 460 at 1 A g^{-1}, 3 420 at 1 A g^{-1}, 3 345 at 1 A g^{-1}, 3	15.1/36900	

References

1. Q. Liang, L. Ye, Z. H. Huang, Q. Xu, Y. Bai, F. Kang, Q. H. Yang, *Nanoscale* **2014**, 6,13831.
2. T. T. Lin, W. H. Lai, Q. F. Lu, Y. Yu, *Electrochem. Acta* **2015**, 178, 517.
3. X. M. Fan, C. Yu, J. Yang, Z. Ling, J. S. Qiu, *Carbon* **2014**, 70, 130.
4. F. Y. Bana, S. Jayabala, H. N. Limb, H. W. Leec, N. M. Huang, *Ceram. Int*. **2017**, 43, 20.
5. Z. Wen, X. Wang, S. Mao, Z. Bo, H. Kim, S. Cui, G. Lu, X. Feng, J. Chen, *Adv. Mater*. **2012**, 24, 5610.
6. J. Yang, E. Zhang, X. Li, Y. Yu, J. Qu, Z. Z. Yu, *ACS Appl. Mater. Inter*. **2016**, 8, 2297.
7. P. Chen, J. J. Yang, S. S. Li, Z. Wang, T. Y. Xiao, Y. H. Qian, S. T. Yu, *Nano Energy* **2013**, 2, 249.
8. M. Kota, X. Yu, S. Yeon, H. Cheong, H. S. Park, *J. Power Sources* **2016**, 303, 372.
9. D. Yu, C. Chen, G. Zhao, L. Sun, B. Du, H. Zhang, Z. Li, Y. Sun, F. Besenbacher, M. Yu. *ChemSusChem*. **2018**, doi: 10.1002/cssc.201800202.
10. J. Hao, Y. Huang, C. He, W. Xu, L. Yuan, D. Shu, X. Song, T. Meng. *Sci Rep*. **2018**, 8(1):562
11. M. Qian, Y. Wang, F. Xu, W. Zhao, T. Lin, F. Huang. *ACS Appl Mater Interfaces*. **2018**,10(1):381-388.
12. C. Liu, J. Liu, J. Wang, J. Li, R. Luo, J. Shen, X. Sun, W. Han, L. Wang. *J. Colloid Interface Sci*. **2018**, 512:713-721.